**PREPARED FOR THE U.S. DEPARTMENT OF ENERGY,
UNDER CONTRACT DE-AC02-76CH03073**

PPPL-3490
UC-70

PPPL-3490

Ohmic Flux Consumption During Initial Operation of the NSTX Spherical Torus

by

J. Menard, B. LeBlanc, S.A. Sabbagh, M. Bell, R. Bell, E. Fredrickson,
D. Gates, S. Jardin, S. Kaye, H. Kugel, R. Maingi, R. Maqueda,
D. Mueller, S. Paul, C.H. Skinner, D. Stutman,
and the NSTX Research Team

October 2000

PPPL
PRINCETON PLASMA PHYSICS LABORATORY

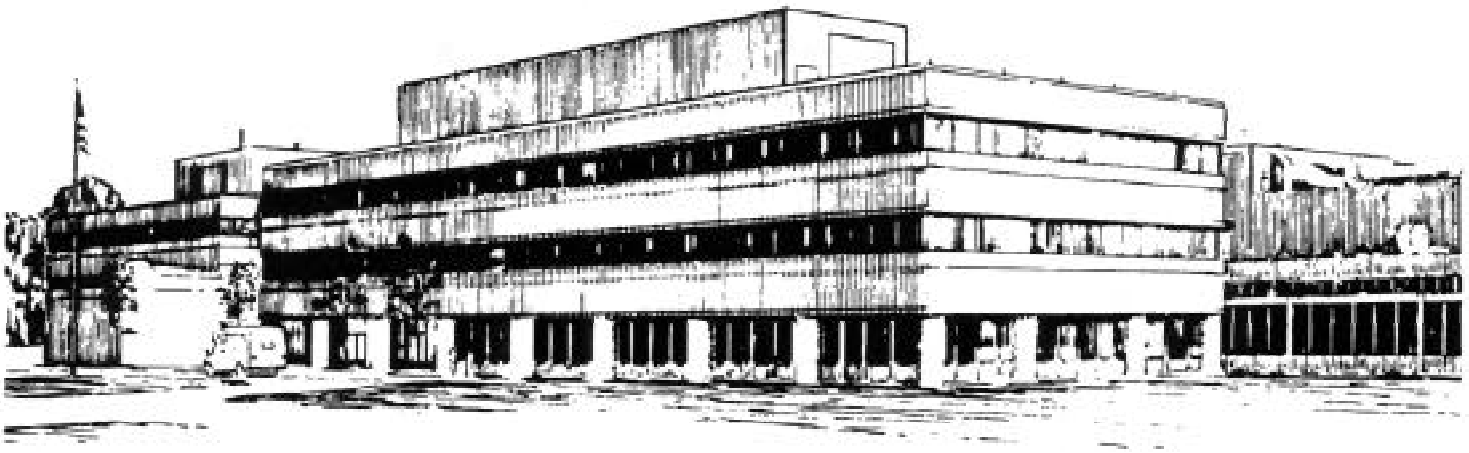

**PRINCETON PLASMA PHYSICS LABORATORY
PRINCETON UNIVERSITY, PRINCETON, NEW JERSEY**

PPPL Reports Disclaimer

Availability

This report is posted on the U.S. Department of Energy's Princeton Plasma Physics Laboratory Publications and Reports web site in Calendar Year 2000. The home page for PPPL Reports and Publications is: http://www.pppl.gov/pub_report/

DOE and DOE Contractors can obtain copies of this report from:

U.S. Department of Energy
Office of Scientific and Technical Information
DOE Technical Information Services (DTIS)
P.O. Box 62
Oak Ridge, TN 37831

Telephone: (865) 576-8401

Fax: (865) 576-5728

Email: reports@adonis.osti.gov

This report is available to the general public from:

National Technical Information Service
U.S. Department of Commerce
5285 Port Royal Road
Springfield, VA 22161

Telephone: 1-800-553-6847 or
(703) 605-6000

Fax: (703) 321-8547

Internet: http://www.ntis.gov/ordering.htm

Ohmic Flux Consumption During Initial Operation of the NSTX Spherical Torus

J. Menard[1], B. LeBlanc[1], S.A. Sabbagh[2], M. Bell[1], R. Bell[1], E. Fredrickson[1], D. Gates[1], S. Jardin[1], S. Kaye[1], H. Kugel[1], R. Maingi[3], R. Maqueda[4], D. Mueller[1], M. Ono[1], S. Paul[1], C.H. Skinner[1], D. Stutman[5], and the NSTX Research Team.

[1]Princeton Plasma Physics Laboratory, Princeton, NJ, USA
[2]Columbia University, New York, NY, USA
[3]Oak Ridge National Laboratory, Oak Ridge, TN, USA
[4]Los Alamos National Laboratory, Los Alamos, NM, USA
[5]Johns Hopkins University, Baltimore, MD, USA

Abstract. The spherical tokamak (ST), because of its slender central column, has very limited volt-second capability relative to a standard aspect ratio tokamak of similar plasma cross-section. Recent experiments on the National Spherical Torus Experiment (NSTX) have begun to quantify and optimize the ohmic current drive efficiency in a MA-class ST device. Sustainable ramp-rates in excess of 5MA/sec during the current rise phase have been achieved on NSTX, while faster ramps generate significant MHD activity. Discharges with I_P exceeding 1MA have been achieved in NSTX with nominal parameters: aspect ratio A=1.3-1.4, elongation κ=2-2.2, triangularity δ=0.4, internal inductance l_i=0.6, and Ejima coefficient C_E=0.35. Flux consumption efficiency results, performance improvements associated with first boronization, and comparisons to neoclassical resistivity are described.

1. Introduction

Spherical tokamak (ST) plasmas [1] have received considerable attention due to encouraging experimental results [2–4] from the Small Tight Aspect Ratio Tokamak (START) [5] and promising theoretical predictions regarding stability [6–9] and confinement [10]. The long-term goal of ST research is the development of steady-state configurations with high plasma β and a high fraction of bootstrap current. The compact geometry of the ST greatly limits the inductive heating and current drive capability of the ohmic heating (OH) solenoid, so the development of non-inductive current drive is crucial to the success of the concept. Nevertheless, near-term research in the ST will rely on OH current drive to generate target plasmas suitable for strong auxiliary heating to test the stability and confinement characteristics of the ST configuration. Recent experiments on the National Spherical Torus Experiment (NSTX) [11, 12] in the United States have begun to achieve high plasma current ohmically in a MA-class ST device. Typical parameters for present NSTX plasmas are: major radius $R_0 = 85$ cm, minor radius a < 68 cm, aspect ratio A$=R_0/a > 1.26$, elongation $\kappa < 2.2$, triangularity $\delta < 0.5$, vacuum toroidal field $B_T = 0.3$ Tesla at R_0, plasma current $I_P < 1$ MA, and plasma pulse length up to 0.5 seconds. Systematic scans of plasma current ramp-rate have been conducted utilizing several diagnostics and modeling tools to characterize the ohmic current drive efficiency, maximize the achievable plasma current, and to investigate the MHD instabilities observed during NSTX operation. The results of these experiments are described in the following sections. Section 2. briefly reviews the derivation of the equations used for parameterizing flux consumption, Section 3. describes the experimental results including comparisons to theory, and a summary of the results is given in Section 4.

2. Ohmic Flux Consumption

Since the ohmic solenoid flux in the ST configuration is so limited, it is desirable to quantify the relationship between the available solenoid flux, the flux at the plasma surface, and the maximum plasma current and flat-top duration achievable with these fluxes. Two different methods have been used previously to relate the poloidal flux change at the plasma boundary (denoted as $\Delta\Phi_S$) to the toroidal plasma current I_P, and a good summary of the theoretical derivation of both methods can be found in Ref. 13.

2.1. The Axial Method

The first method discussed here is commonly called the axial method [14] and was first utilized in analysis of the PLT tokamak. In this method, the change in poloidal flux at the plasma surface is split into inductive (I) and resistive (R) parts:

$$\Delta\Phi_S(t) = \Delta\Phi_I^a(t) + \Delta\Phi_R^a(t) \quad (1)$$

where

$$\Delta\Phi_I^a(t) = \Delta\Psi(t,1) - \Delta\Psi(t,0) \quad (2)$$

and

$$\Delta\Phi_R^a(t) = \Delta\Psi(t,0). \quad (3)$$

Here $\Psi = 2\pi\psi = 2\pi R A_\phi$ is the total poloidal flux integrated from the axis of symmetry of the tokamak (R=0), $\Delta\Psi(t) \equiv \Psi(t) - \Psi(t=0)$, and 0,1 are coordinates referring to the location of the magnetic axis and last-closed flux surface, respectively. The inductive flux difference $\Delta\Phi_I^a$ scales as R_0 and I_P and can be expressed in terms of a dimensionless internal inductance h_i according to:

$$\Delta\Phi_I^a = \frac{h_i \mu_0 R_0 I_P}{2}. \quad (4)$$

The inductance parameter h_i does depend on the poloidal field profile and plasma cross-section shape, but if these effects are taken into account, scaling $\Delta\Phi_I^a$ from one device to another is straight forward.

The resistive flux change $\Delta\Phi_R^a(t)$ is simply the negative time integral of the toroidal loop voltage at the magnetic axis. In so far as the on-axis loop voltage is proportional to the local resistivity, this is a useful (albeit local) measure of resistive flux consumption. In the present study, the EFIT code [15, 16] is routinely used to reconstruct the time evolution of NSTX plasma equilibria, and in principle the on-axis poloidal flux evolution can be followed. Unfortunately, internal magnetic field profile measurements were unavailable for these studies and the experimentally small $\Delta\Phi_R^a(t)$ from unconstrained EFITs does not always vary monotonically in time in the reconstructions. Such considerations motivate the more commonly used Poynting method described in the next section.

2.2. The Poynting Method

The most commonly used method of flux consumption analysis was first applied to the Doublet III device by Ejima [17]. This method is derived from a global electromagnetic power balance using the poloidal field (PF) portion of Poynting's theorem. Ignoring the time evolution of the negligible electric field energy density, power conservation dictates:

$$P_{Poynting} = P_I + P_R, \quad (5)$$

where

$$P_{Poynting} = -\int \frac{\vec{E}_\phi \times \vec{B}_P}{\mu_0} \cdot d\vec{S}, \quad (6)$$

$$P_I = \int \frac{\partial}{\partial t}\left(\frac{B_P^2}{2\mu_0}\right) dV, \quad (7)$$

$$P_R = \int J_\phi E_\phi dV, \quad (8)$$

and the volume of integration is taken to be the volume over which $\vec{J}_{Plasma} \neq 0$, i.e. the plasma volume. Here the poloidal and toroidal magnetic fields have been expressed as $\vec{B}_P = \nabla\psi \times \nabla\phi$ and $\vec{B}_\phi = F(\psi)\nabla\phi$, and the other fields have been expressed in terms of these components. As discussed in Reference 13, if the toroidal field (TF) coil current is held fixed by the TF power supply, the supply must do work against the back-EMF induced by the increasing toroidal flux of a paramagnetic plasma and net power from the TF supply crosses the plasma boundary. For NSTX plasmas which can be strongly paramagnetic by the end of the current ramp, the inductive TF power is non-negligible but is still only a small fraction of the PF heating power. This TF inductive term has been explicitly subtracted from the full Poynting's theorem in deriving Equation 5, as one is generally interested in the poloidal flux change required to generate a given plasma current.

In non-axisymmetric systems or during periods of large-scale MHD activity when axisymmetry is violated, only the total system energy is conserved and the above separation of Poynting's theorem into orthogonal field components is no longer strictly possible. In addition, some care must be taken in interpreting Equation 5, as radiation from the plasma volume is clearly included by Poynting's theorem and must be accounted for. However, any plasma species which is radiating must first have been heated resistively. Thus, plasma stored energy increases, conductive and convective losses, and radiation are all naturally included in the resistive power dissipation term $P_R = \int J_\phi E_\phi dV$.

Using the definitions of flux and field above and assuming the plasma boundary shape is held constant, it can be shown that $P_{Poynting}$ is equivalent to $I_P V_S$ where the surface voltage $V_S \equiv -\frac{d}{dt}\Phi_S$. In general, the plasma boundary shape can evolve considerably during the ramp-up phase and $P_{Poynting}$ can

deviate from $I_P V_S$. This deviation can lead to significant errors in calculations of the instantaneous ohmic heating power, but generally has a smaller impact on calculations of the flux consumed at the end of the current ramp. However, to maintain energy conservation, all subsequent calculations use a modified surface voltage defined by $V_S \equiv P_{Poynting}/I_P$. The total poloidal flux change at the plasma surface can then be expressed as:

$$-\Delta\Phi_S(t) \equiv \int_0^t V_S dt' = \Delta\Phi_I(t) + \Delta\Phi_R(t) \tag{9}$$

where

$$\Delta\Phi_I(t) = \int_0^t \frac{dt'}{I_P} \int \frac{\partial}{\partial t}\left(\frac{B_P^2}{2\mu_0}\right) dV \tag{10}$$

and

$$\Delta\Phi_R(t) = \int_0^t \frac{dt'}{I_P} \int J_\phi E_\phi dV. \tag{11}$$

In devices such as NSTX which have a small gap between the ohmic heating solenoid and the inner-most portion of the plasma boundary, the total flux-swing capability of the OH solenoid ($\Delta\Phi_{OH}$) is nearly equal to $\Delta\Phi_S$. Therefore, the relationship between $\Delta\Phi_S$ and I_P determinines the ultimate toroidal current carrying capability of the device. Because the change in flux at the magnetic axis is small during the current ramp, the change in the surface flux itself is proportional to I_P and R_0, and all three parameters can be related through a dimensionless internal inductance parameter $C \equiv \Delta\Phi/\mu_0 R_0 I_P$ computed at the end of the current ramp. By convention, the resistive flux consumption is parameterized with the Ejima coefficient $C_E \equiv \Delta\Phi_R/\mu_0 R_0 I_P$, and the total surface flux consumption is parameterized here using the Ejima-Wesley coefficient $C_{E-W} \equiv (\Delta\Phi_I + \Delta\Phi_R)/\mu_0 R_0 I_P$ [18]. For all the analysis that follows, EFIT equilibrium solutions were used to compute the volume and time integrals in Equations 10 and 11 explicitly.

Equations 9–11 above indicate that minimizing $J_\phi E_\phi$ with low resistivity and minimizing the volume-integrated B_P^2 by operating with a hollow current profile minimizes the total flux requirement for obtaining a given plasma current. However, the minimum internal inductance of the plasma is limited by MHD stability considerations, and in practice the ramp-rate of the plasma current is balanced against the resistive relaxation of the current profile to obtain the optimal current distribution. Thus, both the Ejima coefficient and the I_P ramp-rate at which it is obtained are required to make a legitimate comparison of the resistive flux dissipation of different devices.

3. Experimental Results

As discussed in the introduction, maximizing the duration of the current sustainment phase to provide target plasmas suitable for auxiliary heating is especially challenging at low aspect ratio. Since significant ohmic flux is consumed prior to the sustainment phase, plasma initiation and current ramp-up are very important phases of any tokamak discharge, and Reference 19 provides an early comprehensive review of this topic.

3.1. Plasma Initiation

Several criteria must be met simultaneously to achieve efficient tokamak initiation. First, a source for generating free electrons during the breakdown phase greatly improves breakdown reliability, and NSTX routinely uses both a biased electron-emitting filament and 10kW of 18GHz (first harmonic) ECH power to facilitate plasma breakdown at D_2 prefill pressures of 20-50 mPa. Second, a good poloidal field null is needed in the vacuum chamber to maximize the field-line connection length to the chamber walls. Work on both JET [20] and DIII-D [19] has shown that reliable current channel formation (without ECH pre-ionization) occurs if the poloidal field in the null region satisfies:

$$\frac{E_\phi B_\phi}{B_P} > 1 kV/m. \tag{12}$$

Since both E_ϕ and B_ϕ scale as 1/R, this criterion is most easily satisfied at small major radius. Thus, even though the stray poloidal field magnitude during breakdown in NSTX is pre-programmed to be less than 20 Gauss over a significant portion of the chamber volume, nearly all NSTX discharges initiate near the central column.

This start-up behavior is evident from Figure 1 which shows the typical evolution of start-up plasmas during the pre-programmed phase using a fast-framing camera [21] in early experiments on NSTX. The OH flux-swing is initiated between t=0-2msec, and a toroidal loop voltage of 4V is present at the surface of the center-stack (CS) casing by t=3-4msec. As seen in the figure, by t=7msec, the current channel has formed and the plasma is growing in volume with decreasing aspect ratio. By t=13msec, a rapid

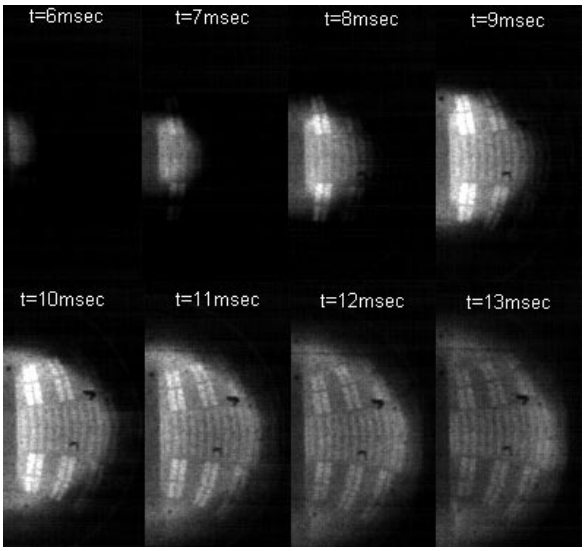

Figure 1. Visible light emission during the start-up phase of shot 100925 on NSTX using the LANL fast-framing camera.

drop in D-alpha light at the plasma boundary (not shown) indicates that the plasma has achieved full ionization. For this particular shot, the plasma has approximately the same aspect ratio and shape that it will have for the remainder of the discharge.

Lastly, the poloidal field curvature and magnitude after current channel formation must be consistent with vertical stability and radial force balance. In NSTX, the vessel toroidal eddy current can be as large as 300kA and can easily exceed the plasma current early during the ramp-up. Two independent eddy current codes [22, 23] have been used to accurately simulate this phase of the discharge to achieve efficient start-up, and both indicate that the criterion of Equation 12 has been satisfied at breakdown over a radial width spanning approximately 40cm from the surface of the central column.

3.2. Plasma current ramp-rate scans

As discussed in Section 2., flux consumption optimization is effectively equivalent to balancing the plasma current ramp-rate against the resistive relaxation of the current profile to obtain the broadest current profile that is stable to ramp-terminating MHD activity. Obviously, plasmas with different resistive dissipation require different ramp-rates to achieve the same current profile at the end of the ramp. Thus, the ability to modify the ramp-rate and control the plasma shape during the ramp is essential, especially at high plasma current. Without the recently implemented digital plasma control system (PCS) [24], achievement of the fast ramps discussed below would have been extremely difficult.

Figure 2 shows the plasma current waveforms obtained during an early I_P ramp-rate scan on NSTX. For each discharge shown in the figure, the OH, PF, and TF coil currents are pre-programmed during the first 20msec of the discharge. At t=20msec, provided that the plasma current has reached a threshold value of 100kA, coil power supply control is turned over to the plasma control system for subsequent I_P, radial position, and vertical position feedback control. The requested I_P after t=20msec was systematically increased to achieve increasingly faster ramps, and the PF shaping coil current ratios were adjusted to compensate for the higher natural elongation caused by the lower internal inductance of the faster ramps.

The systematic scans discussed above showed that sustainable average ramp-rates in excess of 5MA/sec during the current rise phase are possible in NSTX, while significantly faster ramps experience significant MHD activity. As seen in Figure 2, signatures of several different types of MHD events are apparent in the I_P traces. All ramp-rates scanned exhibited at least one late upward spike in the plasma current. This Internal Reconnection Event (IRE) [5, 25, 26] is a nearly ubiquitous feature of ST plasmas and was often associated with low loop voltage near the end of the discharge. For the fastest ramp-rates in the scan (6, 8, and 10 requested MA/sec), early large MHD events terminated the ramp and the plasma current seldom exceeded its pre-event value. Slower ramp-rate discharges generally terminated either due to insufficient loop voltage and/or OH flux. The optimal ramp-rate of 5MA/sec was just slow enough to avoid early MHD activity that terminated the current ramp.

EFIT analysis of theses disharges has been used to track the plasma shape, normalized internal inductance l_i, and Ejima coefficients during the ramp-up. The normalized internal inductance used here is defined as:

$$l_i \equiv \frac{\langle B_P^2 \rangle_V}{\langle B_P \rangle_l^2} \tag{13}$$

where

$$\langle B_P^2 \rangle_V \equiv \frac{\int B_P^2 dV}{\int dV}, \tag{14}$$

$$\langle B_P \rangle_l \equiv \frac{\int \vec{B} \cdot d\vec{l}}{\int dl}, \tag{15}$$

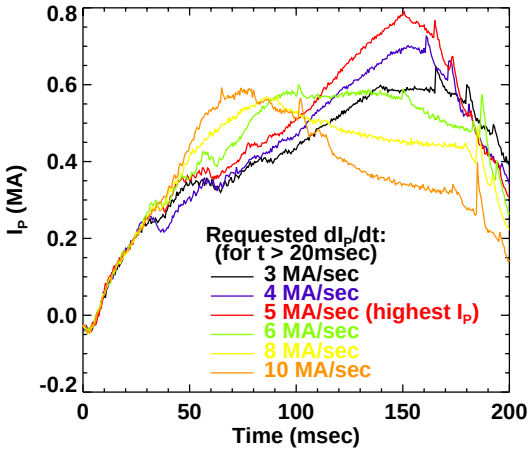

Figure 2. Plasma current traces obtained during a systematic scan of the plasma current ramp-rate.

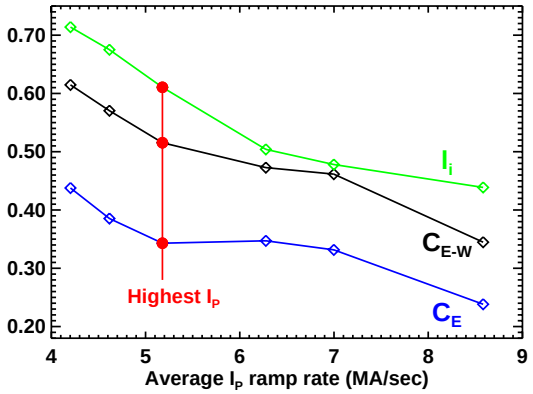

Figure 3. Internal inductance and Ejima coefficients at peak plasma current as a function of I_P ramp-rate for the discharges of Figure 2.

and $\int dV$ and $\int dl$ refer to the plasma volume and plasma boundary poloidal circumference respectively. For the shots shown in Figure 2, the PCS was used to keep the plasma shape inner-wall limited throughout most of the ramp with $A \approx 1.3, \kappa \approx 2 - 2.2$, and $\delta \approx 0.4$. The two highest current discharges in the figure became double-null diverted from t=110 to 150msec. The internal inductance typically increased during these discharges from l_i=0.2-0.3 initially to 0.6-1.0 at the time of maximum current.

Figure 3 shows that the internal inductance at peak current drops by roughly 40% as the average ramp-rate doubles from 4 to 8MA/sec. In addition, this figure shows that lower normalized resistive and total flux consumption was achieved with faster ramps. A noteworthy feature of Figure 3 is that even though the internal inductance drops significantly, most of the drop in total flux consumption with increasing ramp-rate comes from a drop in the resistive component. This is because the inductive portion of the total flux is only 30% of the total at the end of the current ramp. This implies that either the resistive consumption is considerably higher at low aspect ratio, that the inductive consumption is always smaller due to the smaller major radius and lower absolute inductance of the ST, or both.

The most relevant C_E value is that obtained at the highest I_P, and for early NSTX experiments in deuterium, shots optimized for minimal flux consumption had C_E = 0.4-0.45 and C_{E-W} = 0.5-0.6. For comparison, for low loop voltage ramp-up to I_P=1MA in the DIII-D tokamak [19], dI_P/dt = 1-1.5MA/sec, C_E= 0.5 and C_{E-W}=0.9. Values similar to these have been predicted for ITER [27] using the Tokamak Simulation Code (TSC) [28]. Thus, while low aspect ratio tokamaks do have considerably less solenoid flux available, the lower C_{E-W} parameter found in NSTX does imply that some of this loss is recovered in the ST configuration because the inductive flux required to reach a given plasma current is reduced.

3.3. Initial high current discharges

The highest plasma current achieved during the initial phase of NSTX operation was 1MA. Implementation of the full OH capability of NSTX and partial vacuum vessel bake-out were crucial in reaching this physics goal. Plasma parameters at peak I_P from EFIT reconstructions were: A=1.28, κ=1.9, δ=0.4, l_i=0.7, C_E=0.4, and C_{E-W}=0.55. One of the more interesting aspects of the 1MA shots is the reproducible plasma current "hesitation" observable on the experimental I_P traces shown in Figure 4 near t=60msec. Operationally it was found that 1MA could only be achieved by forcing this MHD event to occur early by ramping faster than 5MA/sec. This allowed the plasma to recover in such a way that no subsequent MHD was excited until the late reconnection events which occur after t=170msec. Plasma current ramp-rates both faster and slower than 7MA/sec again led to ramp-terminating MHD activity (see Figure 6). The hesitation event in Figure 4 consumed a significant fraction (20%) of the OH flux and clearly reduced the achievable I_P flattop duration. An important finding evident from Figure 3 and from analysis of the shots in Figure 4 is

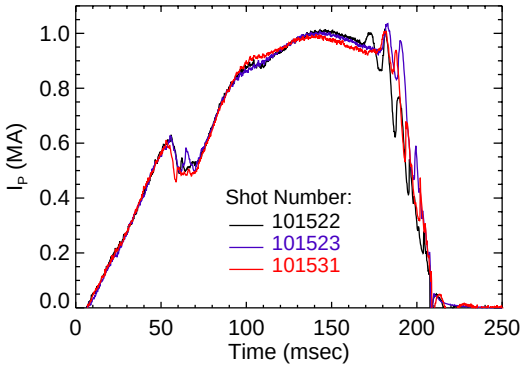

Figure 4. Plasma current traces for 1MA discharges from initial experiments in NSTX.

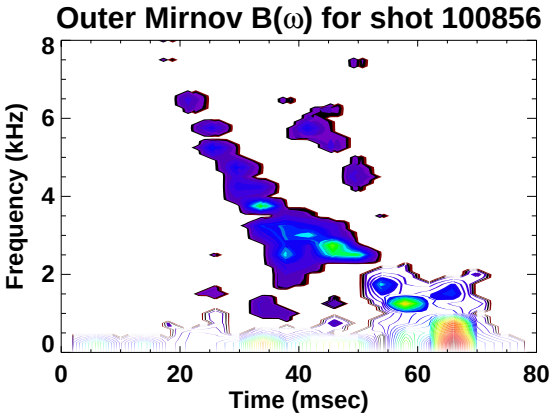

Figure 5. Outboard Mirnov frequency spectrum during the ramp-up phase of shot 100856.

that Ejima coefficients in the expected range of 0.4 were only obtained with relatively fast I_P ramps even after (partial) vessel bake-out. Several possible dissipation mechanisms responsible for this are discussed below.

3.3.1. Tearing activity

Many NSTX discharges exhibited coherent m=2 Mirnov fluctuations with decreasing mode frequency early in the plasma current rise-phase. This behavior may be indicative of the formation of locked (possibly double) tearing modes, and such modes may have dissipated OH flux during the ramp-up in many NSTX discharges. Figure 5 shows the frequency spectrum of a Mirnov sensor on the outboard mid-plane during the early phase of the 8MA/sec discharge of Figure 2 (shot 100856). The mode frequency clearly decreases from 6kHz shortly after breakdown and approaches zero within 40msec, apparently locks, and then grows rapidly near t=65msec. Not every discharge exhibits such strong locking behavior, although many show at least indications of such activity. Better density control, a slower current ramp-rate, and slower plasma expansion during the pre-programmed phase have all been tried with some success to eliminate these modes. Locked mode detector coils are presently being installed to better characterize the modes.

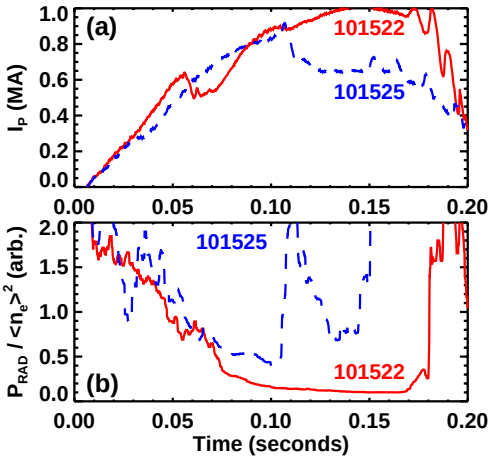

Figure 6. (a) Plasma currents for a 1 MA shot and a failed 1 MA attempt (b) Density-normalized radiated power traces.

3.3.2. Resistivity

The most obvious dissipation mechanism is plasma resistivity, and aside from the predicted neoclassical enhancement of the parallel resistivity due to increased particle trapping, soft X-ray and bolometer signals often showed an emission profile highly peaked on axis in the energy band dominated by metallic impurities. Figure 6 compares plasma current and density-normalized radiated power traces for a successful 1 MA discharge and a 1 MA attempt which failed due to a delayed early MHD event. The only difference between these two shots is the early time history of the requested I_P which modified the applied loop voltage after t=30 msec. The 850 kA peak plasma current trace (shot 101525) in Figure 6a indicates a reconnection event at t=103 msec, and Figure 6b shows that a potentially important difference between these shots is the significant decrease in the density-normalized radiated power of shot 101522 after its first MHD event. This is in contrast to the rapid rise in radiated power after the first event of shot 101525. EFITs (using only

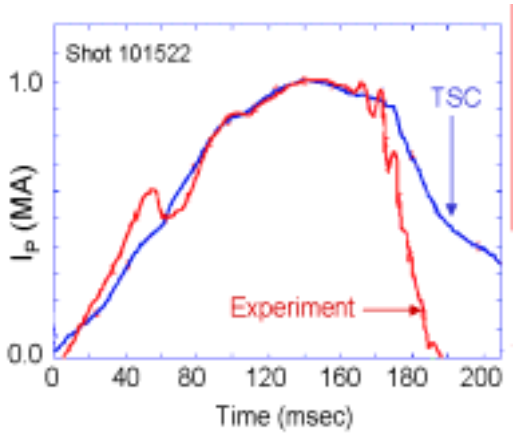

Figure 7. Comparison of experimental and TSC simulated plasma current for a 1MA shot.

external magnetics) suggest q(0) is near 2 just after the events in both discharges in Figure 6, and it is likely that these events are caused by m=2 tearing modes. One plausible interpretation of Figure 6 is that forcing the reconnection event to occur early allowed some fraction of the core impurities to be expelled without destroying the subsequent confinement.

3.3.3. Comparisons to TSC

Because NSTX is a very new device, many of the experiments described in this article were performed without the benefit of profile diagnostics typical of a more mature machine. However, the TSC code was used extensively during the design phase of NSTX and has recently been used to simulate the evolution of NSTX ohmic plasmas. For NSTX applications, TSC uses experimental coil currents and line-density as inputs and uses the resistivity and transport models described in detail in Reference 29. Comparisons between the experimentally measured poloidal fluxes, plasma current, and vessel current and values predicted by TSC generally show good agreement indicating that TSC can be used as a rough diagnostic of plasma parameters.

Figure 7 shows the measured and simulated plasma current from TSC for a 1MA discharge. While there is clearly disagreement between experiment and simulation during early and late periods of strong MHD activity, there is good agreement during the high-current quiescent phase of the discharge. The TSC results were obtained by assuming a flat Z_{eff} profile with an initial value of 2.5 ramping to a final value of 3.6 at peak plasma current. Since the radiated power data in Figure 6b suggests that

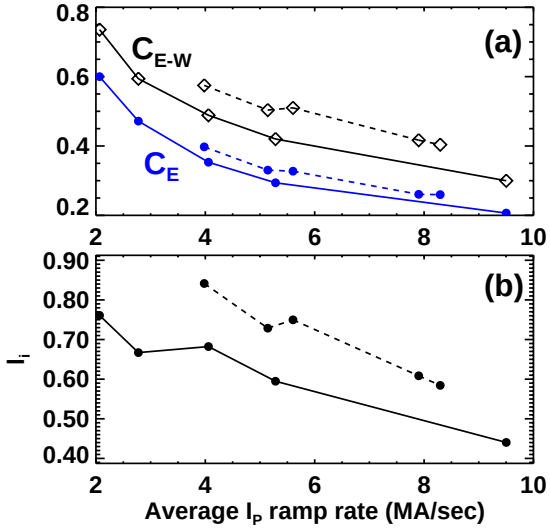

Figure 8. (a) Comparison of Ejima and Ejima-Wesley coefficients versus ramp-rate in deuterium before (dashed lines) and after (solid lines) boronization. (b) Comparison of internal inductance before and after boronization.

101522 should have comparatively fewer impurities, TSC simulations indicate that most other shots in this shot range (and earlier) likely have $Z_{eff} > 3.6$. Lastly, as for the EFIT reconstructions, the central q predicted by TSC crosses 2 near t=55msec, further supporting the idea that m=2 tearing modes are playing a role in the early "hesitation" events of the 1MA discharges.

3.4. Flux consumption post-boronization

In the interest of reducing impurity influxes in NSTX, several device and operational improvements were made following the experiments described in Section 3.3. First, all plasma facing metal surfaces were covered with graphite tiles. Second, the CS and passive plate graphite tiles were baked to 350 and 150°C, respectively. Finally, a 5% trimethyl-boron, 95% helium glow was performed to boronize the machine. As a result of the boronization, visible Oxygen II light emission was reduced by a factor of ten and Carbon III light by a factor of two during subsequent discharges [30].

Such changes in the plasma impurity levels should have an immediate impact on resistive flux consumption, and Figure 8 shows the Ejima coefficients and internal inductance versus I_P ramp-rate for inner-wall limited deuterium plasmas before and after boronization. For both scans, the line-average density at peak I_P was approximately $1-3\times10^{13}cm^{-3}$

and κ varied from 1.8 to 2.1. As seen in Figure 8a, the total surface flux consumption parameter C_{E-W} was reduced by 15-20%, and a similar fractional drop in the internal inductance is shown in Figure 8b. On the other hand, the resistive surface flux consumption parameter C_E dropped by only roughly half this amount. Since most of the resistive power dissipation occurs at large minor radius, Figure 8 may indicate that boronization most strongly impacted the resistivity in the plasma core.

3.4.1. Comparison to neoclassical theory

Just prior to first boronization on NSTX, initial multi-pulse Thomson scattering (MPTS) data became available for selected shots. The present MPTS system fires at 30Hz and has 10 spatial channels with 7-8 channels typically inside the boundary of a ramp-up plasma. By fitting the MPTS data to poloidal flux functions, using recent formulas for the neoclassical conductivity in general geometry and collisionality regime [31], and using smoothed electric fields computed from the EFIT reconstructions, it is possible to compute the expected neoclassical toroidal current density.

Details of the profile of the neoclassical current density cannot be accurately obtained at the present time. However, it is possible to compare the measured and neoclassical Ejima coeffcients and total current, as these quantities are effectively smoothed by volume integration. The neoclassical Ejima coefficient can be obtained from the experimental data using

$$\Delta\Phi_R^{neo}(t) = \int_0^t \frac{dt'}{I_P} \int J_\phi^{neo} E_\phi dV \qquad (16)$$

where J_ϕ^{neo} is obtained from $\langle \vec{J} \cdot \vec{B} \rangle = \sigma^{neo} \langle \vec{E} \cdot \vec{B} \rangle$ and the equilibrium constraint. Then, assuming a flat impurity density profile, the time evolution of $Z_{\rm eff}$ can be inferred from iteratively forcing the neoclassical plasma current and Ejima coefficient to match the measured values at each time step while keeping $Z_{\rm eff} \geq 1$. Once the time history of the estimated $Z_{\rm eff}$ has been computed, a ramp-average can be computed for a particular shot by using $\int J_\phi^{neo} E_\phi dV$ as a weighting function during the current ramp-up.

Using the discharges from Figure 8 where Thomson data was available, Figure 9a shows that the ramp-average $Z_{\rm eff}$ is above unity for all ramp-rates and impurity conditions tested in deuterium. Ignoring bootstrap current, this implies that the measured resistive flux consumption is consistent with neoclassical resistivity. Further, the ratio of the two curves

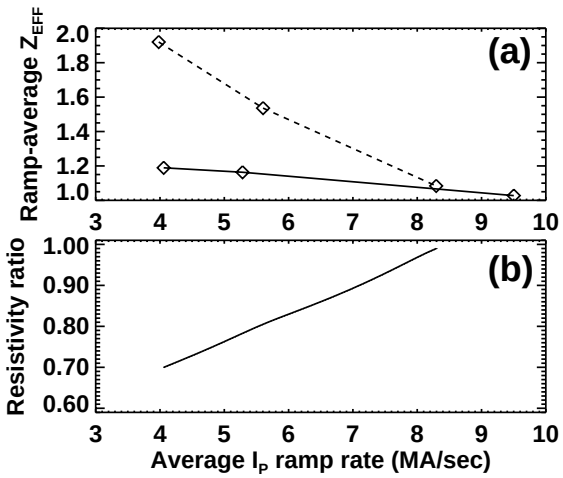

Figure 9. (a) Ramp-average best-fit effective ion charge versus ramp-rate in deuterium before (dashed lines) and after (solid lines) boronization. (b) Estimated ratio of post to pre-boronization resistivity using the data in (a).

in Figure 9a is computed in Figure 9b and indicates that the ramp-average $Z_{\rm eff}$ was reduced by 10-30% after boronization. This drop apparently explains the flux consumption reduction evident in Figure 8.

While the results of this analysis indicate that neoclassical resistivity can explain the flux consumption data, some caveats remain. First, the $Z_{\rm eff}$ estimates will need to be compared to measurements once calibrated visible bremsstrahlung data becomes available. Second, the best-fit $Z_{\rm eff}$ estimates in Figure 9a are systematically low at high average ramp-rate, possibly indicating the generation of runaways. Lastly, because of the high edge safety factor (q_{95}=7-20) and modest core (300-400eV) and edge (30-80eV) electron temperatures of the ramp-up plasmas, the electron collisionality ν_{e*} [31] is typically larger than one in the core and edge and less than one only between r/a $\approx$ 0.4-0.8. Thus, the competing effects of large trapped particle fraction and enhanced electron collisionality provide a challenging test of neoclassical theory.

3.4.2. Performance Improvements

Finally, the reduction in total flux consumption made possible by improvements in machine conditioning and the plasma control system has allowed the achievement of NSTX plasma currents exceeding 1MA without MHD events during the current-rise phase and 800kA discharges with 100msec flat-top durations. Figure 10 shows the I_P waveforms for two such discharges. Both discharges ramp to peak

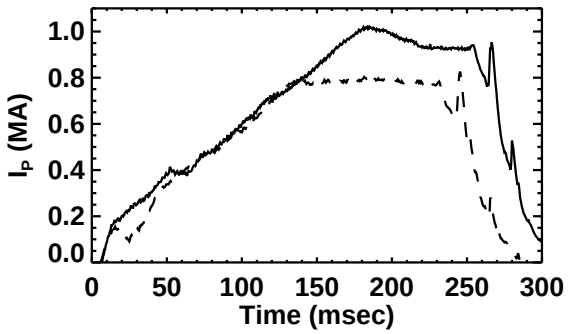

Figure 10. 1MA (solid-103431) and 800kA flat-top (dashed-103026) discharges obtained in NSTX after boronization.

current at just under 6MA/sec and have already been used as targets capable of absorbing significant neutral beam injection power. Future boronization and machine conditioning will hopefully aid in obtaining flat-tops at even higher plasma current values.

4. Summary

The compact geometry of the ST greatly limits the inductive heating and current drive capability of the ohmic heating (OH) solenoid. To best utilize the available solenoid flux, the plasma start-up in NSTX has been optimized and systematic scans of the plasma current ramp-rate have been used to determine the fastest ramp which is stable to MHD activity. Stable ramp-rates in the range of 5-6MA/sec appear to be optimal under present operating conditions, although slower ramps may be required in the future as impurity levels and current penetration rates are further reduced.

The Poynting method originally developed by Ejima has been utilized to quantify poloidal flux consumption in NSTX. With improved machine conditioning and boronization, total flux consumption parameterized by the Ejima-Wesley coefficient C_{E-W} has dropped from 0.55 to 0.45 for ramp-rates of 5MA/sec, and resistive flux consumption parameterized by the Ejima coefficient C_E has dropped from 0.4 to 0.3. High current discharges with I_P=1MA have been achieved in NSTX with nominal parameters: A=1.3-1.4, κ=2-2.2, δ=0.4, l_i=0.6, and Ejima coefficient C_E=0.35. TSC simulations are in good agreement with experimental magnetics data from early NSTX discharges and indicate that Z_{eff} was likely quite large prior to full graphite tile coverage and boronization. In addition, both EFIT and TSC indicate that the plasma current "hesitation" event in the pre-boronization 1MA discharges was coincident with q(0) passing through 2 and suggest that m=2 tearing modes were likely playing a role in limiting the plasma current ramp-rate.

Thomson scattering data has recently become available and has allowed a direct comparison of measured Ejima coefficients to those expected from neoclassical theory. Analysis finds that to within approximately 20% uncertainty, neoclassical resistivity can explain the observed resistive flux consumption and that the average ion charge dropped by 10-30% following first boronization – consistent with the flux consumption studies. This analysis therefore also indicates that while early locked tearing activity may be present in NSTX discharges, such activity is apparently not strongly increasing the dissipation, although the impact of such modes on electron thermal confinement is presently unknown. Future work will concentrate on more accurate calculations of neoclassical resistivity to include multiple ion species effects, and this work coupled with impurity data should eventually allow determination of the fraction of non-inductive current drive.

Finally, the present work has really only addressed the surface flux change required to build up the plasma current, but has dealt little with the requirements for long flat-top duration and profile equilibration. Clearly, early electron heating and/or current drive may provide a means to conserve poloidal flux [12] and extend plasma pulse lengths, but profile equilibration times would also be longer in these hotter plasmas. As for high aspect ratio tokamaks, steady state operation will ultimately require a significant fraction of the plasma current to come from the neoclassical bootstrap current.

Acknowledgements

Steve Sabbagh and Ben LeBlanc are especially acknowledged for providing the EFIT reconstructions and Thomson scattering data which made the majority of the analysis in this paper possible. This work was supported by the United States Department of Energy under contract numbers DE-AC02-76CH03037 (PPPL), DE-AC05-00R22725 (ORNL), W-7405-ENG-36 (LANL) and grant numbers DE-FG02-99ER54524 (CU), DE-FG02-99ER54523 (JHU).

References

[1] PENG, Y.-K. M. and STRICKLER, D. J., Nucl. Fus. **26** (1986) 769.

[2] SYKES, A., AKERS, R., APPEL, L., CAROLAN, P., CONNOR, J., et al., Phys. Rev. Lett. **84** (2000) 495.

[3] GATES, D. A., AKERS, R., APPEL, L., CAROLAN, P. G., CONWAY, N., et al., Phys. Plasmas **5** (1998) 1775.

[4] GRYAZNEVICH, M., AKERS, R., CAROLAN, P. G., CONWAY, N. J., GATES, D., et al., Phys. Rev. Lett. **80** (1998) 3972.

[5] SYKES, A., DELBOSCO, E., COLCHIN, R., CUNNINGHAM, G., DUCK, R., et al., Nucl. Fus. **32** (1992) 694.

[6] MENARD, J. E., JARDIN, S. C., KAYE, S. M., KESSEL, C. E., and MANICKAM, J., Nucl. Fus. **37** (1997) 595.

[7] MILLER, R. L., LIN-LIU, Y. R., TURNBULL, A. D., CHAN, V. S., PERLSTEIN, L. D., et al., Phys. Plasmas **4** (1997) 1062.

[8] KRUGER, S. E., HEGNA, C. C., and CALLEN, J. D., Phys. Plasmas **5** (1998) 455.

[9] PAOLETTI, F., SABBAGH, S. A., GATES, D., KAYE, S. M., MANICKAM, J., et al., Impact of profile variation on the equilibrium and stability of NSTX, in *25th European Conference on Controlled Fusion and Plasma Physics*, p. 1709, Maastricht, The Netherlands, 1999, European Physical Society.

[10] REWOLDT, G., TANG, W. M., KAYE, S., and MENARD, J., Phys. Plasmas **3** (1996) 1667.

[11] ONO, M., KAYE, S., PENG, Y.-K., BARNES, G., BLANCHARD, W., et al., Nucl. Fus. **40** (2000) 557.

[12] KAYE, S., ONO, M., PENG, Y.-K., BATCHELOR, D., CARTER, M., et al., Fus. Technol. **36** (1999) 16.

[13] HOULBERG, W. A., Nucl. Fus. **27** (1987) 1009.

[14] HAWRYLUK, R. J., BOL, K., and JOHNSON, D., Nucl. Fus. **19** (1979) 1519.

[15] SABBAGH, S. A., KAYE, S. M., MENARD, J., BELL, M., BELL, R., et al., Equilibrium properties of spherical torus plasmas in NSTX, IAEA 2000, submitted to Nuclear Fusion.

[16] LAO, L. L., St. John, H., STAMBAUGH, R. D., KELLMAN, A. G., and PFEIFFER, W., Nucl. Fus. **25** (1985) 1611.

[17] EJIMA, S., CALLIS, R., LUXON, J., STAMBAUGH, R., TAYLOR, T., et al., Nucl. Fus. **22** (1982) 1313.

[18] WESLEY, J., BELJAKOV, V., BULMER, R., HOGAN, J., KAISER, T., et al., The ITER poloidal field system, in *Plasma Physics and Controlled Nuclear Fusion Research 1990*, volume 3 of *Thirteenth conference proceedings*, p. 421, Washington, DC, 1991, International Atomic Energy Association, Vienna.

[19] LLOYD, B., JACKSON, G., TAYLOR, T., LAZARUS, E., LUCE, T., et al., Nucl. Fus. **31** (1991) 2031.

[20] TANGA, A., THOMAS, P., CORDEY, J., CHRISTIANSEN, J., EJIMA, S., et al., *Tokamak Start-up*, p. 159, Plenum Press, New York, 1986.

[21] MAQUEDA, R. and WURDEN, G., Nucl. Fus. **39** (1999) 629.

[22] MENARD, J. E., LRDIAG code, private communication, 2000.

[23] HATCHER, R. E., LRSIM code, private communication, 2000.

[24] GATES, D., MUELLER, D., NEUMEYER, C., and FERRON, J., Control system development plan for the National Spherical Torus eXperiment, in SCHALLER, S., editor, *Eleventh IEEE NPSS Real Time Conference*, 1999.

[25] ONO, M., STUTMAN, D., HWANG, Y.-S., CHOE, W., MENARD, J., et al., Investigation of the effect of resistive MHD modes on spherical torus performance in CDX-U, in *Fusion Energy 1996*, volume 2 of *Sixteenth conference proceedings*, p. 71, Montreal, Canada, 1997, International Atomic Energy Association, Vienna.

[26] MIZUGUCHI, N., HAYASHI, T., and SATO, T., Phys. Plasmas **7** (2000) 940.

[27] JARDIN, S. C., KESSEL, C. E., and POMPHREY, N., Nucl. Fus. **34** (1994) 1145.

[28] JARDIN, S. C., POMPHREY, N., and DELUCIA, J., J. Comput. Phys. **66** (1986) 481.

[29] JARDIN, S. C., BELL, M. G., and POMPHREY, N., Nucl. Fus. **33** (1993) 371.

[30] SKINNER, C., Private communication, to be published in Nuclear Fusion.

[31] SAUTER, O., ANGIONI, C., and LIN-LIU, Y. R., Phys. Plasmas **6** (1999) 2834.

The Princeton Plasma Physics Laboratory is operated
by Princeton University under contract
with the U.S. Department of Energy.

Information Services
Princeton Plasma Physics Laboratory
P.O. Box 451
Princeton, NJ 08543

Phone: 609-243-2750
Fax: 609-243-2751
e-mail: pppl_info@pppl.gov
Internet Address: http://www.pppl.gov